


RESEARCH

Open Access



# Performance analysis of spatial multiplexing MIMO-MFSK based on energy detection for fast-fading environments

Shuaijun Li<sup>1,2</sup>, Hongbing Qiu<sup>1</sup>, Lin Zheng<sup>1,2\*</sup>  and Chao Yang<sup>1</sup>

\*Correspondence:  
gwzheng@gmail.com

<sup>1</sup> Key Laboratory of Cognitive Radio and Information Processing, Ministry of Education, Guilin University of Electronic Technology, Guilin 541004, China  
<sup>2</sup> Science and Technology on Communication Networks Laboratory, Shijiazhuang 050081, Hebei, China

## Abstract

In fast-fading scattering environments such as high-speed rail and low-altitude communications, mobile communication systems need to quickly and robustly estimate and equalize fast-fading, time-varying channels. Under these circumstances, noncoherent multiple-input multiple-output (MIMO) has received attention in recent years, since it is less influenced by factors such as phase fluctuations and has fewer requirements for channel estimation and synchronization. Spatial multiplexing MIMO-MFSK based on energy detection is different from conventional noncoherent MIMO in that it can achieve higher spatial multiplexing gain in the independent distribution of channel fading statistics. At the receiver, partial real channel state information (CSI) is available, which can improve the capacity while ensuring the reliability of the link. With partial real CSI replacing instantaneous CSI, the system performance is inferior to conventional coherent MIMO under the influence of noise. As a result, it is necessary to analyze its theoretical detection performance. By energy detection, the noise of the MIMO-MFSK system conforms to the generalized gamma distribution. On the basis of this distribution, the optimal decision rule of the system and the symbol error rate (SER) formula are derived. Additionally, we investigate the signal-dependent noise problem of minimum Euclidean distance detection. Numerical results show that the SER formula fits well with the simulation results under the condition of a high signal-to-noise ratio.

**Keywords:** Noncoherent MIMO, Multiple frequency-shift keying (MFSK), Energy detection, Generalized gamma distribution, SER

## 1 Introduction

As high-speed railways, low-altitude communication, and other vehicles have higher requirements for communication quality, the issue of highly reliable and large-capacity communication in fast-fading environments has gradually attracted attention. In fast-fading scenarios, a number of high-reliability and low-latency applications, including driverless, high-definition video, and video conferencing, are difficult to implement. Furthermore, the IMT-2020 standard does not provide low-complexity noncoherent measures to address the above issues.

The IMT-2020 standard divides 5G into three main application scenarios: enhanced mobile broadband (eMBB), massive machine type communications (mMTC), and

ultra-reliable low-latency communications (uRLLC). The uRLLC need to meet the requirements of high reliability, low latency, and high mobility. It can provide more stable services and lower transmission delays for high-speed mobile users, with an end-to-end delay of in the order of 1 ms. Nevertheless, channel estimation causes partial transmission delay in coherent communication, and pilot symbols occupy a portion of the time and frequency slots. Moreover, the complexity of the channel estimation increases as the number of antennas and users grows, which ultimately increases the system delay. To avoid pilot pollution, channel estimation must also use orthogonal training sequences. Further, in fast-fading environments, the channel coherence time reduces and the channel fading coefficient changes faster, so that instantaneous channel estimation is difficult. Contrary to coherent systems, noncoherent systems have the advantages of low complexity, low power consumption, simple circuit design, insensitivity to channel changes, and can achieve higher spectral efficiency [1]. In this paper, we describe a spatial multiplexing MIMO-MFSK system based on energy detection. It can replace instantaneous channel state information (iCSI) with partial real CSI.

Noncoherent MIMO is insensitive to time-varying channels, and the receiving equipment is simple, which has become one of the main research fields of MIMO in recent years. The noncoherent MIMO research area primarily focuses on Grassmannian MIMO [2–6], differential detection MIMO [7–10], and energy detection MIMO [16–22]. Among them, Grassmannian MIMO demands no or only partial CSI for demodulation, which applies to high SNR and fast-fading scenarios [2]. However, the capacity of Grassmannian MIMO is limited by channel coherence time and complex encoding [3]. Additionally, systematic unitary space–time codes have relatively high design and decoding complexity [4], and their decoding complexity increases exponentially with increasing bit transmission rates [5]. Noncoherent MIMO with differential detection could also reduce the dependence on the channel information. Differential space–time modulation is a noncoherent MIMO scheme that does not require accurate CSI [7]. As an extended form of differential phase-shift keying modulation in a multi-antenna system, this method uses the phase difference between two adjacent transmission blocks to transmit the information and completes the communication without CSI [8–10]. Regrettably, differential detection necessitates a quasi-static fading channel with consistent channel states between adjacent symbols, which is not always possible in fast-fading environments.

The Doppler shift brought about by fast-fading will cause the phase of the far-field MIMO channel to change rapidly. Due to the lack of CSI, conventional noncoherent MIMO systems are unable to meet the requirements in fast-fading environments in terms of detection performance, channel utilization efficiency, and resistance to fast time-varying fading. Existing noncoherent MIMO systems aim at reducing the reliance on channel information, and most designs are based on quasi-static channel conditions. Signal processing and detection algorithms are implemented in spatial diversity, so the multiplexing efficiency of the system is relatively low. In [11], space–time–frequency coding is designed based on MFSK, which uses the soft information of the preceding and following symbols to perform multi-level energy likelihood detection. It does not need CSI, only needs to receive symbol energy and noise variance information, and can provide space–time–frequency diversity gain. Diversity technology recently developed

will help 5G new radio systems achieve better theoretical performance [12]. In addition, MIMO with energy detection of spatial multiplexing has been gaining attention due to its performance improvement [13], which can increase communication capacity while also ensuring reliability.

Up to now, MIMO based on energy detection has been one of the hot research topics in the region of noncoherent communication. The modulation methods mainly include multi-ary amplitude-shift keying (ASK), frequency-shift keying (FSK), and pulse-amplitude modulation (PAM) [14, 15]. Motivated by the simplicity of the circuit design and low-complexity signal detection, a nonlinear MIMO system using amplitude detection and phase detection is proposed, which is robust to noise [16]. Goldsmith proposed a noncoherent SIMO scheme that does not use the iCSI but rather only the knowledge of the channel statistics, a transmitter that modulates information only in the amplitude of the symbols, and a receiver that measures only the average received energy across the antennas [17–19]. [20] generalizes the constellation design in [17] for arbitrary numbers of users and channel conditions. Inspired by the seminal work [18], the authors proposed new joint multi-user constellation designs in massive MIMO systems that are asymptotically optimal for symbol error rate [21]. [22] proposed a massive MIMO transmission scheme with full frequency reuse for low earth orbit satellite communication systems, utilizing statistical CSI to overcome the difficulty of obtaining iCSI. Besides this, multiple novel communication schemes are also introduced to reduce mutual interference and external jamming attacks in fading scenarios. Fast frequency-hopping with MFSK is a widespread noncoherent communication scheme used in military communication systems [23]. In [24], a frequency-hopping multiaccess system with frequency-shift keying modulation was presented. The bit error rate performance of these investigated hopping patterns imposed in multi-node Internet-of-Thing systems is evaluated by simulations.

Currently, MIMO based on energy detection is mainly considered from the perspective of an infinite number of receiving antennas and mostly uses amplitude modulation with limited modulation space. In this situation, the interference from the receiving antenna is treated as system noise, and the receiving path is asymptotically orthogonal. Moreover, most research studies based on energy detection methods use a SIMO system architecture and statistical channel characteristics to perform diversity signal processing [17–19]. There is a lack of research on spatial multiplexing techniques for noncoherent MIMO in fast time-varying channels without CSI or with partial CSI. Prior work initially analyzed the MIMO-MFSK model with a limited number of antennas and extended the modulation space to the frequency dimension [25]. Afterward, we equivalent the system model through nonlinear processing and perform noncoherent detection using equivalent channel parameters. A theoretical expression for the average SER and the optimal decision rule of the system is deduced. However, for the high complexity of maximum likelihood (ML) detection with optimal judgment, ML is simplified through multi-antenna joint minimum Euclidean distance detection. Simultaneously, the distribution problem of signal-dependent noise associated with minimum Euclidean distance detection is investigated.

## 2 Method

The methodology of this paper is presented as follows. We first describe a spatial multiplexing MIMO-MFSK system for high reliability and large-capacity communication in fast-fading environments. Then, the system is equated to a real linear model by a non-linear treatment of the square-law energy detection. Under the linear model, we provide the mathematical expressions for equivalent signal, equivalent channel, and equivalent noise, respectively, and deduce the mean vector and covariance matrix of the equivalent noise. Subsequently, we analyze the probability distribution of the noise after energy detection and the theoretical performance of the system. Following that we present a suboptimal signal detection method and discuss the signal-dependent noise problem. Finally, we perform numerical simulations.

## 3 Channel environment

For a communication system with  $N_t$  transmitting and  $N_r$  receiving antennas, the channel conforms to the typical Rice channel characteristics in the context of fast-fading line-of-sight (LOS) environments as communication transmission applications [26]. The channel  $\mathbf{H}(t)$  at the transmitter and receiver can be divided into LOS and diffuse portions. Assuming the LOS component is in a static phase with uniform phase distribution. There is

$$\mathbf{H}(t) = \sqrt{1-a}\mathbf{H}^s(t) + a\mathbf{H}^d(t), \quad (1)$$

where  $\mathbf{H}^s(t)$  denotes the LOS portion of the channel,  $\mathbf{H}^d(t)$  represents the scattering portion and the  $a$  represents the channel weighting coefficient. When  $a = 1$ , the received signal is the multipath scattering component of the transmitted signal, and the channel model is the Rayleigh channel. When  $a = 0$  or  $a \ll 1$ , the received signal is regarded as the LOS part of the transmitted signal, and the channel characteristics tend to be stable [27].

Considering a far-field environment where the antenna array size is much smaller than the propagation distance, it can be deemed that all concurrent transmission channels of the system experience approximately the same Doppler shift. Furthermore, even though the Doppler shift for each space division path is slightly different due to different direction angles, the effect is not very obvious. In high-speed railways and low-altitude communication systems, where the direct path is extremely powerful, this is still true [28]. The Doppler shift is mainly reflected in the phase change of channel  $\mathbf{H}(t)$ , that is

$$e^{j\varphi_{l,n}(t)} = e^{j2\pi f_D^{l,n}(t)} = e^{j2\pi f_D(t)} = e^{j\varphi(t)}, \quad (2)$$

where  $f_D^{l,n}$  represents the Doppler shift from the  $n$ th transmitting antenna to the  $l$ th receiving antenna.

At  $a = 0$  or  $a \ll 1$ ,  $\mathbf{H}(t) \approx \mathbf{H}^s(t)$ , that is

$$\mathbf{H}(t) \approx \mathbf{H}^s(t) = e^{j\varphi(t)} \begin{bmatrix} h_{11}e^{j\theta_{11}} & \cdots & h_{1N_t}e^{j\theta_{1N_t}} \\ \vdots & h_{ln}e^{j\theta_{ln}} & \vdots \\ h_{N_r1}e^{j\theta_{N_r1}} & \cdots & h_{N_rN_t}e^{j\theta_{N_rN_t}} \end{bmatrix} = \begin{bmatrix} \mathbf{h}_1 \\ \vdots \\ \mathbf{h}_{N_r} \end{bmatrix}, \quad (3)$$

where  $\mathbf{h}_l$  is the  $l$ th row of  $\mathbf{H}(t)$  for  $l = 1, \dots, N_r$ . The fading coefficient  $h_{ln}e^{j\theta_{ln}}$  is assumed to follow independent and identically distributed (i.i.d.) complex Gaussian distribution with zero mean and unit variance, there is

$$h_{ln}e^{j\theta_{ln}} \sim \mathcal{CN}(0, 1). \quad (4)$$

The Doppler shift is supposed to be approximately constant within one symbol period of the transmitted signal, and it is shown that

$$e^{j\varphi(t)} = e^{j\varphi}. \quad (5)$$

Assume that the frequency modulation signal  $e^{j2\pi f_1 t + \varphi_1}$  performs square-law energy detection at frequencies  $f_1$  and  $f_2$ , respectively. At the same time, the  $f_1 - f_2 = \frac{1}{T}$  ( $T$  is the duration of a symbol), the frequencies are orthogonal to each other, we have

$$\mathbb{Z}_1 = \left| \frac{1}{T} \int_0^T e^{j2\pi f_1 t + \varphi_1} e^{-j2\pi f_1 t} dt \right|^2 = |e^{j\varphi_1}|^2 = 1 \quad (6)$$

$$\mathbb{Z}_2 = \left| \frac{1}{T} \int_0^T e^{j2\pi f_1 t + \varphi_1} e^{-j2\pi f_2 t} dt \right|^2 = \left| e^{j\varphi_1} \frac{\sin[\pi(f_1 - f_2)T]}{\pi(f_1 - f_2)T} e^{j\pi(f_1 - f_2)T} \right|^2 = 0. \quad (7)$$

The result of energy detection of the  $e^{j2\pi f_1 t + \varphi_1}$  at a frequency matching its frequency point is one. Otherwise, the result is zero. Through square-law processing, the random phase interference from the carrier is eliminated. Meanwhile, the orthogonal signal characteristic minimizes signal interference. Thus, it has the characteristics of anti-Doppler frequency offset and phase offset in fast-fading environments. Additionally, the Doppler shift will also cause the signal frequency offset, which can be ignored under the condition that the Doppler frequency deviation is far less than the symbol rate.

## 4 System model

### 4.1 Spatial multiplexing MIMO-MFSK system

Consider the spatial multiplexing MIMO-MFSK system with  $N_t$  transmit and  $N_r$  receive antennas, shown in Fig. 1.

After V-BLAST encoding, the transmitted data stream is modulated with MFSK, upconverted, and sent in parallel through multiple transmitting antennas. At the receiving end, the transmitted signal is received in a noncoherent manner. Within a symbol interval, the  $N_r \times 1$  received signal vector (i.e.,  $\mathbf{Y} = [y_1, y_2, \dots, y_{N_r}]^T$ ) is represented by

$$\mathbf{Y} = \mathbf{H}\mathbf{s} + \mathbf{n}, \quad (8)$$

where  $\mathbf{H}$  is the  $N_r \times N_t$  channel matrix (i.e.,  $\mathbf{H} = [\mathbf{h}_1, \mathbf{h}_2, \dots, \mathbf{h}_{N_r}]^T$ ),  $\mathbf{s}$  is the  $N_t \times 1$  transmitted information-bearing symbol vector through MFSK, and  $\mathbf{n}$  is the  $N_r \times 1$  AWGN vector (i.e.,  $\mathbf{n} = [n_1, n_2, \dots, n_{N_r}]^T$ ), which is independent of the channel matrix  $\mathbf{H}$ . The AWGN vector  $n_1, n_2, \dots, n_{N_r}$  are i.i.d., each follows a complex Gaussian distribution with mean 0 and variance  $\sigma_n^2$ , i.e.,  $\mathcal{CN}(0, \sigma_n^2)$ .

The  $w$ th symbol of the  $n$ th transmitting antenna through MFSK modulation is denoted as

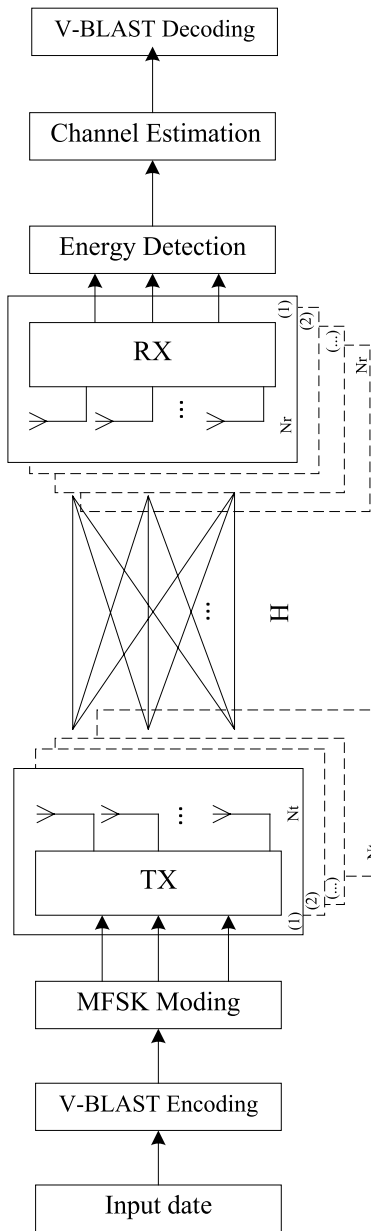


**Fig. 1** Block diagram of spatial multiplexing MIMO-MFSK based on energy detection. The figure shows the processing of the system

$$s_{nw}(t) = e^{j2\pi f_{b_{nw}}t}, \quad (9)$$

where  $f_{b_{nw}}$  denotes the frequency of the  $w$ th symbol on the  $n$ th transmitting antenna, and  $b_{nw} = \{0, 1, \dots, M-1\}$  indicates the transmitted symbol mapped by V-BLAST encoding. Moreover, the modulated information-bearing symbol matrix is

$$\mathbb{S} = \begin{bmatrix} s_{11}(t) & \cdots & s_{1N}(t) \\ \vdots & s_{nw}(t) & \vdots \\ s_{N_t1}(t) & \cdots & s_{N_tN}(t) \end{bmatrix} = [\mathbf{s}_1, \mathbf{s}_2, \dots, \mathbf{s}_n, \dots, \mathbf{s}_N], \quad (10)$$

where  $N$  denotes the number of symbols transmitted,  $\mathbf{s}_n$  represents the  $n$ th column of the sending symbol matrix.

#### 4.2 Equivalent real linear model by energy detection

The  $w$ th symbol received by the  $l$ th receiving antenna in a symbol interval is recorded as

$$\begin{aligned} y_{lw} &= \mathbf{h}_l \mathbf{s}_w + n_{lw} \\ &= \sum_{n=1}^{N_t} h_{ln} e^{j\theta_{ln}} e^{j\varphi} s_{nw}(t) + n_{lw}(t). \end{aligned} \quad (11)$$

The  $y_{lw}$  performs energy detection after frequency correlation at  $f_i$ ,  $i = [1, \dots, M]$ , we get

$$\begin{aligned} r_{l,f_i} &= \left| \frac{1}{T} \int_0^T y_{lw}(t) e^{-j2\pi f_i t} dt \right|^2 \\ &= |\mathbf{h}_l \mathbf{X}_{w,f_i} + v_{lw}|^2 \\ &= \left| \sum_{n=1}^{N_t} h_{ln} e^{j\theta_{ln}} e^{j\varphi} X_{nw,f_i} \right|^2 + 2\text{Re} \left( v_{lw}^* \sum_{n=1}^{N_t} h_{ln} e^{j\theta_{ln}} e^{j\varphi} X_{nw,f_i} \right) + |v_{lw}|^2, \end{aligned} \quad (12)$$

where  $\mathbf{X}_{w,f_i} = [X_{1w,f_i}, X_{2w,f_i}, \dots, X_{N_t w,f_i}]^T$ ,  $\mathbf{X}_{w,f_i}$  is the result of  $\mathbf{s}_w$  through correlation at  $f_i$ , according to (6) and (7),  $X_{nw,f_i} \in (0, 1)$ . The  $\text{Re}(\cdot)$  stands for the real part of a complex number. Additionally, the equivalent noise component by energy detection is

$$u_l = 2\text{Re} \left( v_{lw}^* \sum_{n=1}^{N_t} h_{ln} e^{j\theta_{ln}} e^{j\varphi} X_{nw,f_i} \right) + |v_{lw}|^2, \quad (13)$$

where  $v_{lw}$  is the result of  $n_{lw}$  through correlation at  $f_i$ ,  $i = [1, \dots, M]$ . Since frequencies are orthogonal to each other,  $v_{lw}$  is independent of each other at each frequency and follows a complex Gaussian distribution, i.e.,  $v_{lw} \sim \mathcal{CN}(0, \frac{\sigma_n^2}{M})$ .

The equivalent signal part by energy detection can be obtained as

$$\left| \sum_{n=1}^{N_t} h_{ln} e^{j\theta_{ln}} e^{j\varphi} X_{nw,f_i} \right|^2 = \sum_{n=1}^{N_t} \sum_{j=1}^{N_t} h_{ln} h_{lj} \cos(\theta_{ln} - \theta_{lj}) X_{nf_i} X_{jf_i}. \quad (14)$$

In (14), through square-law processing, the Doppler shift  $e^{j\varphi}$  in fast-fading environments is eliminated. The  $l$ th row vector of the equivalent channel matrix can be expressed as

$$\tilde{\mathbf{h}}_l = [h_{l1}^2, \dots, h_{lN_t}^2, 2h_{l1}h_{l2}\cos(\theta_{l1} - \theta_{l2}), \dots, 2h_{l(N_t-1)}h_{lN_t}\cos(\theta_{l(N_t-1)} - \theta_{lN_t})], \quad (15)$$

and the equivalent transmitting data vector is

$$\tilde{\mathbf{X}}_{w f_i} = [X_{1w f_i}^2, \dots, X_{N_t w f_i}^2, X_{1w f_i}X_{2w f_i}, \dots, X_{(N_t-1)w f_i}X_{N_t w f_i}]^T, \quad (16)$$

where  $X_{n w f_i} \in (0, 1)$ . According to (12)–(16), the transceiver system by energy detection at  $f_i$  can be equivalent to a real linear model, which is given by

$$\mathbf{r}_{f_i} = \tilde{\mathbf{H}}\tilde{\mathbf{X}}_{w f_i} + \mathbf{u}, \quad (17)$$

where  $\mathbf{r}_{f_i}$  is the equivalent receiving data (i.e.,  $\mathbf{r}_{f_i} = [r_{1f_i}, r_{2f_i}, \dots, r_{N_r f_i}]^T$ ),  $\tilde{\mathbf{H}}$  is the equivalent channel matrix (i.e.,  $\tilde{\mathbf{H}} = [\tilde{\mathbf{h}}_1, \tilde{\mathbf{h}}_2, \dots, \tilde{\mathbf{h}}_{N_t}]^T$ ),  $\mathbf{u}$  is the equivalent noise (i.e.,  $\mathbf{u} = [u_1, u_2, \dots, u_{N_r}]^T$ ).

The equivalent noise component is given by (13), furthermore, we have

$$E(u_l) = E[2\text{Re}(v_{lw}^* \sum_{n=1}^{N_t} h_{ln} e^{j\theta_{ln}} e^{j\varphi} X_{n w f_i}) + |v_{lw}|^2] = \frac{\sigma_n^2}{M}, \quad (18)$$

where  $E(\cdot)$  denotes the expectation operator. Since  $r_{l f_i} = |\mathbf{h}_l \mathbf{X}_{w f_i} + v_{lw}|^2$  obeys the generalized gamma distribution, we can further deduce as

$$E(r_{l f_i}) = \tilde{\mathbf{h}}_l \tilde{\mathbf{X}}_{w f_i} + \frac{\sigma_n^2}{M} \quad (19)$$

$$E(r_{l f_i}^2) = (\tilde{\mathbf{h}}_l \tilde{\mathbf{X}}_{w f_i})^2 + \frac{4\sigma_n^2}{M} \tilde{\mathbf{h}}_l \tilde{\mathbf{X}}_{w f_i} + \frac{2\sigma_n^2}{M}, \quad l = 1, 2, \dots, N_r. \quad (20)$$

Therefore, the diagonal and off-diagonal elements of the covariance matrix of the equivalent noise vector  $\mathbf{u}$  are derived as

$$\text{var}(u_l) = E[(r_{l f_i} - \tilde{\mathbf{h}}_l \tilde{\mathbf{X}}_{w f_i})^2] - E^2(u_l) = \frac{2\sigma_n^2}{M} \tilde{\mathbf{h}}_l \tilde{\mathbf{X}}_{w f_i} + \frac{\sigma_n^4}{M^2} \quad (21)$$

$$\text{cov}(u_l, u_k) = E[(r_{l f_i} - \tilde{\mathbf{h}}_l \tilde{\mathbf{X}}_{w f_i})(r_{k f_i} - \tilde{\mathbf{h}}_k \tilde{\mathbf{X}}_{w f_i})] - E(u_l)E(u_k) = 0 \quad (22)$$

$l \neq k, l, k = 1, 2, \dots, N_r,$

where  $\text{var}(\cdot)$  denotes variance operator and  $\text{cov}(\cdot)$  denotes covariance operator.

In summary, the spatial multiplexing MIMO-MFSK system based on energy detection is equivalent to a real linear model, which is written as

$$\mathbf{r} = \tilde{\mathbf{H}}\tilde{\mathbf{X}}_w + \mathbf{u}, \quad (23)$$

where  $\tilde{\mathbf{X}}_w = [\tilde{\mathbf{X}}_{w f_1}, \dots, \tilde{\mathbf{X}}_{w f_M}]$ ,  $\tilde{\mathbf{X}}_w$  is the equivalent data component of the  $w$ th transmit symbol by energy detection at  $M$  frequency points, respectively.



## 5 Detection and performance analysis

Above, we analyzed the spatial multiplexing MIMO-MFSK system and derived the equivalent system model. The performance of noncoherent detection is inferior to conventional coherent detection in the presence of noise and other interference. As a result, we must use the theoretical SER formula as the primary performance metric. In addition, we present a suboptimal signal detection approach.

### 5.1 Theoretical SER for spatial multiplexing MIMO-MFSK system

The MIMO-MFSK system is equivalent to a linear model. Following that we perform a theoretical analysis of the detection performance. The transmitted data stream is mapped to a symbol vector  $c_m$  by V-BLAST encoding, and its signal set is represented as

$$\mathcal{C} = \{c_1, c_2, \dots, c_m, \dots, c_{M_{N_t}}\}, \quad (24)$$

and

$$c_m = [b_1 \cdots b_{N_t}]^T, \quad b_1, \dots, b_{N_t} \in \{0, 1, \dots, M-1\}, \quad (25)$$

where the  $c_m$  is modulated into a frequency modulation signal vector  $\mathbf{s}_m$ , as in (9). According to (6) and (7), the  $\mathbf{s}_m$  is correlated at  $f_i$  to obtain a vector with elements of 0 or 1, that is

$$\mathbf{X}_m = [a_1 \cdots a_{N_t}]^T, \quad a_1, \dots, a_{N_t} \in \{0, 1\}. \quad (26)$$

If the transmission symbol vector is  $c_m$ , it can obtain from (12) that

$$\begin{aligned} r_{l,f_i} &= |\mathbf{h}_l \mathbf{X}_{m,f_i} + v_{lm}|^2 \\ &= \left| \sum_{n=1}^{N_t} h_{ln} e^{j\theta_{ln}} e^{j\varphi} X_{nm,f_i} + v_{lm} \right|^2 \end{aligned}$$

where  $|\mathbf{h}_l \mathbf{X}_{m,f_i} + v_{lm}|$  obeys the Rice distribution. Through the square processing,  $r_{l,f_i}$  conforms to the generalized gamma distribution, which can be written as

$$r_{l,f_i} \sim \text{Gamma}(\alpha, \beta, \lambda) \quad (27)$$

$$\text{where } \alpha = 1, \beta = 2\sigma_n^2/M, \lambda = \left| \sum_{n=1}^{N_t} h_{ln} e^{j\theta_{ln}} e^{j\varphi} X_{nm,f_i} \right|^2.$$

The probability density function of  $r_{l,f_i}$ , as well as the likelihood function, can be indicated as

$$\begin{aligned} f(r_{l,f_i} | \mathbf{h}_l, \mathbf{X}_{m,f_i}) &= \frac{1}{\beta} \left( \frac{r_{l,f_i}}{\lambda} \right)^{(\alpha-1)/2} I_{\alpha-1} \left( \frac{2\sqrt{\lambda r_{l,f_i}}}{\beta} \right) \exp \left( -\frac{r_{l,f_i} + \lambda}{\beta} \right) \\ &= \frac{1}{2\sigma_n^2/M} I_0 \left( \frac{\left| \sum_{n=1}^{N_t} h_{ln} e^{j\theta_{ln}} e^{j\varphi} X_{nm,f_i} \right| \sqrt{r_{l,f_i}}}{\sigma_n^2/M} \right) \exp \left( -\frac{r_{l,f_i} + \left| \sum_{n=1}^{N_t} h_{ln} e^{j\theta_{ln}} e^{j\varphi} X_{nm,f_i} \right|^2}{2\sigma_n^2/M} \right) \end{aligned} \quad (28)$$

where  $I_0(\cdot)$  denotes the modified Bessel function of the zeroth order and the first kind. Owing to the frequencies of MFSK are orthogonal to each other, the likelihood functions at each frequency are independent of each other. Thus, the joint likelihood function is the product of the likelihood functions at each frequency. The  $c_m$  that maximizes the sum of the logarithmic joint likelihood function is the signal that is correctly decided, that is

$$\begin{aligned}\hat{c} &= \arg \max_{c_m \in \mathcal{C}} \sum_{l=1}^{N_r} \sum_{i=1}^M \ln[f(r_{l,f_i} | \mathbf{h}_l, \mathbf{X}_{m,f_i})] \\ &= \arg \max_{c_m \in \mathcal{C}} \sum_{l=1}^{N_r} \sum_{i=1}^M \ln \left( \frac{1}{2\sigma_n^2/M} \right) + \ln \left[ I_0 \left( \frac{\left| \sum_{n=1}^{N_t} h_{ln} e^{j\theta_{ln}} e^{j\varphi} X_{nm,f_i} \right| \sqrt{r_{l,f_i}}}{\sigma_n^2/M} \right) \right] - \frac{r_{l,f_i} + \left| \sum_{n=1}^{N_t} h_{ln} e^{j\theta_{ln}} e^{j\varphi} X_{nm,f_i} \right|^2}{2\sigma_n^2/M}.\end{aligned}\quad (29)$$

Since  $\ln(\frac{1}{2\sigma_n^2/M})$  and  $-\frac{r_{l,f_i}}{2\sigma_n^2/M}$  do not rely on the search parameter  $c_m$ , we remove them from the decision variable. The decision criterion (29) can be written as

$$\hat{c} = \arg \max_{c_m \in \mathcal{C}} \sum_{l=1}^{N_r} \sum_{i=1}^M \ln \left[ I_0 \left( \frac{\left| \sum_{n=1}^{N_t} h_{ln} e^{j\theta_{ln}} e^{j\varphi} X_{nm,f_i} \right| \sqrt{r_{l,f_i}}}{\sigma_n^2/M} \right) \right] - \frac{\left| \sum_{n=1}^{N_t} h_{ln} e^{j\theta_{ln}} e^{j\varphi} X_{nm,f_i} \right|^2}{2\sigma_n^2/M}.\quad (30)$$

Thus, (30) is the optimal decision rule for the MIMO-MFSK system. Since the Bessel function is nonlinear, the implementation complexity of the receiver is high. Approximate processing of the Bessel function at high SNR can simplify the optimal decision rule.  $I_0(\cdot)$  is expanded as

$$I_0(x) \approx \frac{e^x}{\sqrt{2\pi x}} \left[ 1 + \frac{1}{8x} + \frac{1 \times 9}{2!(8x)^2} + \frac{1 \times 9 \times 25}{3!(8x)^3} + \dots \right],\quad (31)$$

when the absolute value of the argument inside  $I_0(\cdot)$  is large,  $\ln[I_0(x)]$  is approximated as

$$\ln[I_0(x)] \approx \ln \left( \frac{e^x}{\sqrt{2\pi x}} \right) \approx x.\quad (32)$$

Applying (32) to (30), the optimal decision rule (30) can be rewritten as

$$\hat{c} = \arg \max_{c_m \in \mathcal{C}} \sum_{l=1}^{N_r} \sum_{i=1}^M \left( 2 \left| \sum_{n=1}^{N_t} h_{ln} e^{j\theta_{ln}} e^{j\varphi} X_{nm,f_i} \right| \sqrt{r_{l,f_i}} - \left| \sum_{n=1}^{N_t} h_{ln} e^{j\theta_{ln}} e^{j\varphi} X_{nm,f_i} \right|^2 \right).\quad (33)$$

The probability of correct decision when the  $c_m \in \mathcal{C}$  is transmitted, denote by  $p_{c_m}$ , is obtained from (33) as

$$\begin{aligned}
p_{c_m} &= p_r \left( \sum_{l=1}^{N_r} \sum_{i=1}^M 2 |\mathbf{h}_l \mathbf{X}_{m_{fi}}| |\mathbf{h}_l \mathbf{X}_{m_{fi}} + v_{lm}| - |\mathbf{h}_l \mathbf{X}_{m_{fi}}|^2 \right. \\
&> \left. \sum_{l=1}^{N_r} \sum_{i=1}^M 2 |\mathbf{h}_l \mathbf{X}_{k_{fi}}| |\mathbf{h}_l \mathbf{X}_{m_{fi}} + v_{lm}| - |\mathbf{h}_l \mathbf{X}_{k_{fi}}|^2 \right) \\
&k \neq m, \quad k = (1 \dots M^{N_t}),
\end{aligned} \tag{34}$$

$$\begin{aligned}
p_{c_m} &= p_r \left( \max_{k \in (1 \dots M^{N_t}) - (m)} \sum_{l=1}^{N_r} \sum_{i=1}^M 2 |\mathbf{h}_l \mathbf{X}_{k_{fi}}| |\mathbf{h}_l \mathbf{X}_{m_{fi}} + v_{lm}| - |\mathbf{h}_l \mathbf{X}_{k_{fi}}|^2 \right. \\
&< \left. \sum_{l=1}^{N_r} \sum_{i=1}^M 2 |\mathbf{h}_l \mathbf{X}_{m_{fi}}| |\mathbf{h}_l \mathbf{X}_{m_{fi}} + v_{lm}| - |\mathbf{h}_l \mathbf{X}_{m_{fi}}|^2 \right)
\end{aligned} \tag{35}$$

Under the high SNR,  $|\mathbf{h}_l \mathbf{X}_{m_{fi}} + v_{lm}|$  in (35) can be processed as follows

$$\begin{aligned}
|\mathbf{h}_l \mathbf{X}_{m_{fi}} + v_{lm}| &= \left\{ |\mathbf{h}_l \mathbf{X}_{m_{fi}}|^2 + 2 \operatorname{Re}[v_{lm} (\mathbf{h}_l \mathbf{X}_{m_{fi}})^*] + |v_{lm}|^2 \right\}^{\frac{1}{2}} \\
&\approx |\mathbf{h}_l \mathbf{X}_{m_{fi}}| \left\{ 1 + \frac{2 \operatorname{Re}[v_{lm} (\mathbf{h}_l \mathbf{X}_{m_{fi}})^*]}{|\mathbf{h}_l \mathbf{X}_{m_{fi}}|^2} \right\}^{\frac{1}{2}},
\end{aligned} \tag{36}$$

the Taylor series expansion of  $\left\{ 1 + \frac{2 \operatorname{Re}[v_{lm} (\mathbf{h}_l \mathbf{X}_{m_{fi}})^*]}{|\mathbf{h}_l \mathbf{X}_{m_{fi}}|^2} \right\}^{\frac{1}{2}}$  is given by

$$\left\{ 1 + \frac{2 \operatorname{Re}[v_{lm} (\mathbf{h}_l \mathbf{X}_{m_{fi}})^*]}{|\mathbf{h}_l \mathbf{X}_{m_{fi}}|^2} \right\}^{\frac{1}{2}} = 1 + \left\{ \frac{\operatorname{Re}[v_{lm} (\mathbf{h}_l \mathbf{X}_{m_{fi}})^*]}{|\mathbf{h}_l \mathbf{X}_{m_{fi}}|^2} \right\} - \frac{1}{4} \left\{ \frac{\operatorname{Re}[v_{lm} (\mathbf{h}_l \mathbf{X}_{m_{fi}})^*]}{|\mathbf{h}_l \mathbf{X}_{m_{fi}}|^2} \right\}^2 + R_n(\cdot), \tag{37}$$

where the  $R_n(\cdot)$  is Lagrangian remainder of Taylor series expansion.

At high SNR, the high-order term of (37) is small and can be ignored. The first two terms of (37) are brought into (36) to obtain as

$$|\mathbf{h}_l \mathbf{X}_{m_{fi}} + v_{lm}| \approx |\mathbf{h}_l \mathbf{X}_{m_{fi}}| + \operatorname{Re}(v_{lm}), \tag{38}$$

where  $\operatorname{Re}(v_{lm})$  follows a Gaussian distribution with mean 0 and variance  $\frac{\sigma_n^2}{2M}$ , that is

$$\operatorname{Re}(v_{lm}) \sim \mathcal{N}\left(0, \frac{\sigma_n^2}{2M}\right). \tag{39}$$

Bring (38) into (35), we get

$$p_{c_m} \approx p_r \left[ \max_{k \in (1 \dots M^{N_t}) - (m)} \sum_{l=1}^{N_r} \sum_{i=1}^M 2 (|\mathbf{h}_l \mathbf{X}_{k_{fi}}| - |\mathbf{h}_l \mathbf{X}_{m_{fi}}|) \operatorname{Re}(v_{lm}) - (|\mathbf{h}_l \mathbf{X}_{k_{fi}}| - |\mathbf{h}_l \mathbf{X}_{m_{fi}}|)^2 < 0 \right]. \tag{40}$$

Define

$$g = \sum_{l=1}^{N_r} \sum_{i=1}^M 2 (|\mathbf{h}_l \mathbf{X}_{k_{fi}}| - |\mathbf{h}_l \mathbf{X}_{m_{fi}}|) \operatorname{Re}(v_{lm}) - (|\mathbf{h}_l \mathbf{X}_{k_{fi}}| - |\mathbf{h}_l \mathbf{X}_{m_{fi}}|)^2, \tag{41}$$

furthermore, the  $g$  follows a Gaussian distribution, there is

$$g \sim \mathcal{N} \left\{ \sum_{l=1}^{N_r} \sum_{i=1}^M -(|\mathbf{h}_l \mathbf{X}_{k_{f_i}}| - |\mathbf{h}_l \mathbf{X}_{m_{f_i}}|)^2, \sum_{l=1}^{N_r} \sum_{i=1}^M \frac{2\sigma_n^2 (|\mathbf{h}_l \mathbf{X}_{k_{f_i}}| - |\mathbf{h}_l \mathbf{X}_{m_{f_i}}|)^2}{M} \right\}. \quad (42)$$

Applying the Gaussian distribution normalized result of (42) to (40), the probability of a correct decision can be represented as

$$p_{c_m} = \phi \left( \sqrt{\min_{k \in (1 \dots M^{N_t}) - (m)} \sum_{l=1}^{N_r} \sum_{i=1}^M \frac{(|\mathbf{h}_l \mathbf{X}_{k_{f_i}}| - |\mathbf{h}_l \mathbf{X}_{m_{f_i}}|)^2}{2\sigma_n^2/M}} \right), \quad (43)$$

where  $\phi(\cdot)$  is the distribution function of the standard Gaussian distribution. The probability of error decision when  $c_m \in \mathcal{C}$  is transmitted, denoted by  $p_{e_m}$ , is given by

$$p_{e_m} = 1 - p_{c_m} = Q \left( \sqrt{\min_{k \in (1 \dots M^{N_t}) - (m)} \sum_{l=1}^{N_r} \sum_{i=1}^M \frac{(|\mathbf{h}_l \mathbf{X}_{k_{f_i}}| - |\mathbf{h}_l \mathbf{X}_{m_{f_i}}|)^2}{2\sigma_n^2/M}} \right), \quad (44)$$

where  $Q(\cdot)$  denotes the Gaussian Q-function. The average SER under equiprobable signaling is obtained as

$$\begin{aligned} p_e &= \frac{1}{M^{N_t}} \sum_{m=1}^{M^{N_t}} p_{e_m} \\ &= \frac{1}{M^{N_t}} Q \left( \sqrt{\min_{k \in (1 \dots M^{N_t}) - (m)} \sum_{l=1}^{N_r} \sum_{i=1}^M \frac{(|\mathbf{h}_l \mathbf{X}_{k_{f_i}}| - |\mathbf{h}_l \mathbf{X}_{m_{f_i}}|)^2}{2\sigma_n^2/M}} \right) \quad m = 1, \dots, M^{N_t}. \end{aligned} \quad (45)$$

## 5.2 Multi-antenna joint minimum Euclidean distance detection

The (30) is the optimal decision rule. It is optimal to use the obeyed distribution to make a decision, but the complexity is high. As a result, it can be simplified by using the minimum of the joint Euclidean distance of multiple antennas at M frequency points under the equivalent linear model, which can be defined as

$$\hat{c} = \underset{m \in (1 \dots M^{N_t})}{\operatorname{argmin}} \sum_{l=1}^{N_r} \sum_{i=1}^M \left| r_{l_{f_i}} - \tilde{\mathbf{h}}_l \tilde{\mathbf{X}}_{m_{f_i}} \right|^2, \quad (46)$$

where  $\tilde{\mathbf{h}}_l$  is the  $l$ th row of  $\tilde{\mathbf{H}}$ ,  $\tilde{\mathbf{H}}$  is an equivalent real channel matrix with the dimension  $N_r \times \frac{N_t(N_t+1)}{2}$  and is a relatively slowly varying partial CSI in the context of fast-fading LOS environments as communication transmission applications. Thus, it is possible to estimate the equivalent real channel under fast-fading environments. As a linear channel matrix, conventional linear channel estimation algorithms can be applied, i.e., least squares channel estimation, there is

$$\hat{\mathbf{H}} = \mathbf{r} \tilde{\mathbf{X}}^T \left( \tilde{\mathbf{X}} \tilde{\mathbf{X}}^T \right)^{-1}, \quad (47)$$

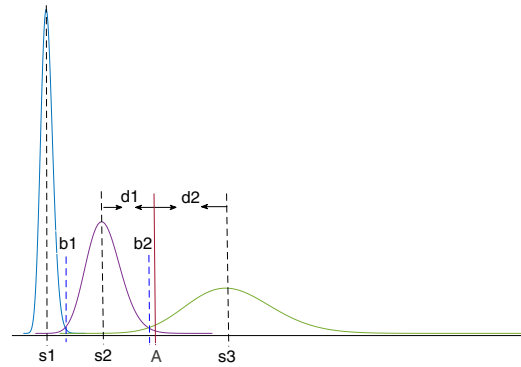


**Fig. 2** Signal-dependent noise distribution at low SNR. The figure shows the distribution of the received signal when the transmitted signal is  $s_1, s_2$  and  $s_3$  at low SNR

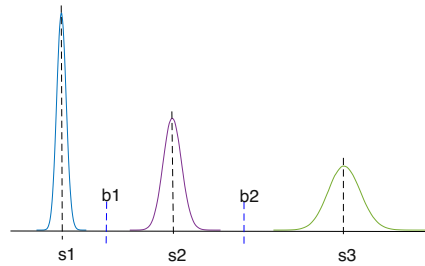


**Fig. 3** Signal-dependent noise distribution at high SNR. The figure shows the distribution of the received signal when the transmitted signal is  $s_1, s_2$  and  $s_3$  at high SNR

where  $\mathbf{r}$  is the received data by energy detection,  $\tilde{\mathbf{X}}$  is the equivalent data using the Hadamard matrix as the training sequence. The equivalent channel  $\tilde{\mathbf{H}}$  in a fast-fading environment is defined by Eq. (15), which is a real channel that contains channel amplitude state information without the fast-varying phase term  $e^{j\varphi}$ . In the general Rice high-speed railways and low-altitude communication channel models, the amplitude term is mainly determined by the attenuation of the direct path, and the motion causes the phase to change rapidly [29, 30]. As a result, the estimation complexity of the equivalent channel  $\tilde{\mathbf{H}}$  is significantly lower than that of the complex channel. When linear detection algorithms such as zero forcing (ZF) and minimum mean square error (MMSE) are adopted, the number of received antennas is constrained by  $N_r \geq \frac{N_t(N_t+1)}{2}$ . To ensure that  $\tilde{\mathbf{H}}$  is invertible and the weighted channel matrix  $(\tilde{\mathbf{H}}^T \tilde{\mathbf{H}})^{-1} \tilde{\mathbf{H}}^T$  can be obtained.

## 6 Results and discussion

Above, we describe a spatial multiplexing MIMO-MFSK system that has Doppler robustness in fast-fading wireless communication environments. The system is then equated to a linear model, and SER is given as the performance metric. Subsequently, we adopted a suboptimal detection method. In this section, the theoretical average SER is compared with the numerical results, and the simulation also demonstrates the accuracy

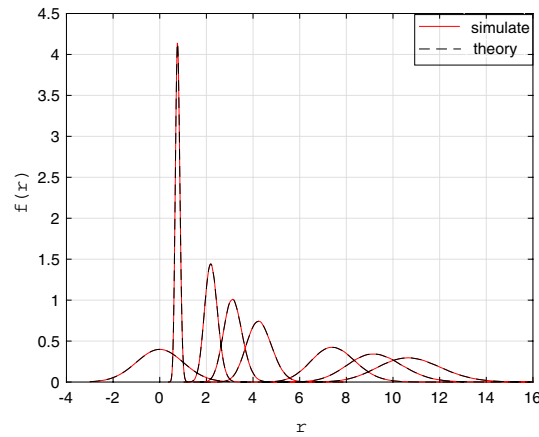


**Fig. 4** The  $f(r_{i,f_i}|\mathbf{h}_i, \mathbf{X}_{f_i})$  of the joint constellation at  $f_i$  under low SNR. The figure compares  $f(r_{i,f_i}|\mathbf{h}_i, \mathbf{X}_{f_i})$  by the theoretical analysis and the simulation at low SNR

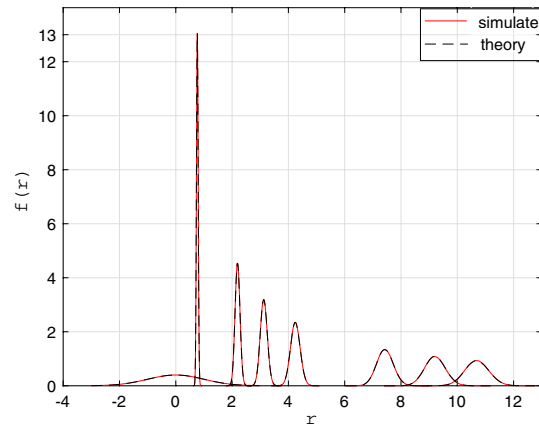


**Fig. 5** The  $f(r_{i,f_i}|\mathbf{h}_i, \mathbf{X}_{f_i})$  of the joint constellation at  $f_i$  under high SNR. The figure compares  $f(r_{i,f_i}|\mathbf{h}_i, \mathbf{X}_{f_i})$  by the theoretical analysis and the simulation at high SNR

of the received signal distribution by energy detection. Additionally, we analyze the signal-dependent noise problem of minimum Euclidean distance detection.

Figures 2 and 3 are the distributions of the received signal after energy detection when the transmitted signal is  $\mathbf{s}_1$ ,  $\mathbf{s}_2$  and  $\mathbf{s}_3$ . The optimal decision rule states that when the received signal falls on the left region of the decision boundary  $b_1$ , the transmitted signal is considered to be  $\mathbf{s}_1$ . A judgment transmitted signal is considered  $\mathbf{s}_2$  as long as the received signal lies between the decision boundaries  $b_1$  and  $b_2$ . When the received signal is in the area to the right of the judgment boundary  $b_2$ , the signal is sent as  $\mathbf{s}_3$ . The variance of each distribution is relatively large at low SNR, so there is obvious overlap between adjacent distributions. At the same time, large noise will cause deviations in the center positions of each distribution, so the distance between their centers will differ from the original distance. The accuracy of the minimum Euclidean distance detection is affected by the above changes. According to the optimal decision rule, the transmitted signal should be determined as  $\mathbf{s}_3$  when the received signal falls at position

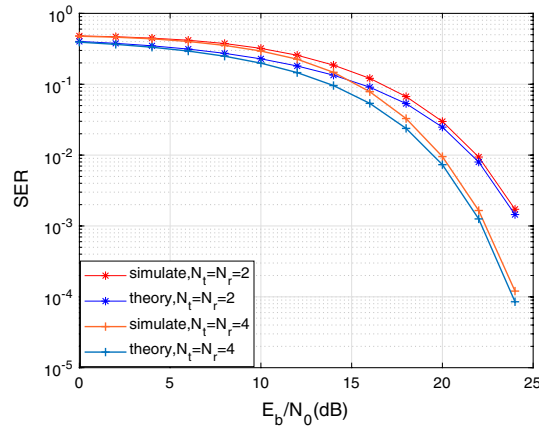


**Fig. 6** Simulation and theoretical comparison of the SER of MIMO-4FSK. In the figure, the SER is compared with the theoretical analysis and the simulation

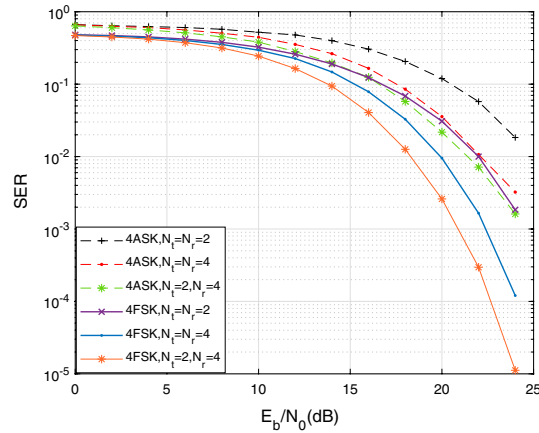


**Fig. 7** SER performance of MIMO-4FSK and MIMO-4ASK under energy detection. The figure compares the performances of two different modulation modes based on energy detection

A. Considering the minimum Euclidean distance, the influence of large noise makes  $d_1 < d_2$ , so it will be misjudged as  $s_2$ . As depicted in Fig. 3, when variance at high SNR is reduced, distributions become more concentrated, and the overlap regions between neighboring distributions become smaller, thus improving the overall performance of minimum Euclidean distance detection. In addition, the isometric constellation design of the transmitting signal can also reduce the overlap regions between neighboring distributions and improve the accuracy of the minimum Euclidean distance detection.

In a MIMO-MFSK system with 3 transmitting and receiving antennas, the transmitted signals are all correlated at  $f_i$  to obtain eight signal vectors, each with elements 0 and 1. Figures 4 and 5 show the comparison between the numerical and theoretical formula (28) of the transmitting signal constellation under low and high SNR. Numerical results show that the simulation and the theoretical formula match well, and as the SNR increases, the overlap regions between adjacent distributions shrink.

Figure 6 compares the numerical results using minimum Euclidean distance detection (46) with the theoretical formula for average symbol error probability (45) in a spatial

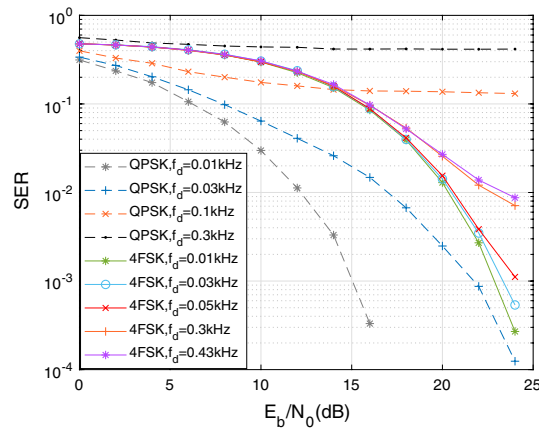


**Fig. 8** SER performance of noncoherent MIMO-4FSK and coherent MIMO-QPSK in fast-fading environments. The figure compares the Doppler robustness of MIMO-4FSK and MIMO-QPSK in fast-fading environments

multiplexing MIMO-4FSK system based on energy detection. At high SNR, the simulation matches the theoretical formulation well. As the number of antennas increases, SER performance improves. The reason is that as the number of receiving antennas increases, the diversity gain of the receiving end will increase as well. In addition, the decision criterion is to adopt multi-antenna joint detection. As the number of antennas increases, the reliability of detection will be enhanced. Thus, the SER of the system will be improved.

Figure 7 shows the performance comparison of the MIMO system using 4FSK and 4ASK modulation. The performance of the MIMO-4ASK system is limited by the limited amplitude modulation space. As a result, the performance of the MIMO-4FSK system outperforms that of the MIMO-4ASK. As the number of receiving antennas increases while the transmitting antenna remains the same, the performance of the system improves. The reason is that the diversity gain of the receiving end will increase as the number of receiving antennas increases. In contrast, the receiving antenna remains the same, and increasing the transmitting antenna will deteriorate performance. The transmit signal is encoded with V-BLAST spatial multiplexing and multiple data streams are sent in parallel. If the diversity gain at the receiver side remains constant and the number of transmitting antennas increases, the mutual interference under spatial multiplexing will increase, and the system performance will deteriorate.

In the context of a fast-fading channel, the frequency band is around 2.4 GHz and the bandwidth is around 1 MHz. As shown in Fig. 8, we describe the Doppler robustness analysis of the spatial 4FSK modulation with energy detection and the spatial QPSK modulation with coherent detection when transmitting and receiving antennas are both 4. The performance of MIMO-QPSK deteriorates sharply as the Doppler shift increases. In a fast-fading environment, the channel changes rapidly and the channel coherence time becomes shorter, which makes instantaneous channel estimation difficult. Coherent detection will rapidly degrade if there is no instantaneous tracking of phase changes. In comparison, the MIMO-4FSK based on energy detection has better Doppler robustness. Square-law energy detection can eliminate phase interference so that it has little effect



on the energy detection system. If the Doppler shift is large, the signal frequency will be offset, resulting in a frequency mismatch, which directly affects the error performance.

## 7 Conclusion

This paper presents a spatial multiplexing MIMO-MFSK system based on energy detection with a limited number of transceiver antennas, further extending the modulation space to mutually orthogonal amplitude and frequency dimensions. In fast-fading environments, it can improve communication capacity while maintaining reliability. The energy detection technique can help avoid phase synchronization problems, reduce the complexity of the training sequence, and eliminate pilot pollution. As a result, the system will be more robust to Doppler effects. The MIMO-MFSK system is equivalent to a real linear model through nonlinear processing, which reduces channel estimation and signal detection complexity. As the primary metric for judging system performance, the theoretical expression for the SER is given, and we analyze the problem of signal-dependent noise that affects the detection performance of the system. To further enhance overall system performance, future work can optimize the constellation design according to the SER formula.

### Abbreviations

MIMO	Multiple-input multiple-output
SER	Symbol error rate
SNR	Signal-to-noise ratio
eMBB	Enhanced mobile broadband
mMTC	Massive machine type communications
uRLLC	Ultra-reliable low-latency communications
CSI	Channel state information
iCSI	Instantaneous channel state information
ASK	Amplitude-shift keying
MFSK	Multiple frequency-shift keying
PAM	Pulse-amplitude modulation
SIMO	Single-input multiple-output
AWGN	Additive white Gaussian noise
ML	Maximum likelihood
LOS	Line-of-sight
ZF	Zero forcing
MMSE	Minimum mean square error
iid	Independent and identically distributed

### Acknowledgements

The authors would like to thank the editor and the anonymous reviewers for their helpful comments and suggestions.

### Authors' contributions

All authors made contributions in the discussions, analyses, and implementation of the proposed solution. LSJ drafted the manuscript. All authors read and approved the final manuscript.

### Funding

This work was supported in part by the National Natural Science Foundation of China (61571143), in part by the Fund Project of key Laboratory of Cognitive Radio and Information Processing, Ministry of Education (CRKL200102), in part by the Natural Science Foundation of Guangxi in China (2020GXNSFAA159067), and partly supported by fund of Science and Technology on Communication Networks Laboratory (SCX20641X001).

### Availability of data and materials

Not applicable.

### Declarations

#### Competing interests

The authors declare that they have no competing interests.

Received: 6 September 2021 Accepted: 21 March 2022

Published: 4 April 2022

**References**

1. RH Gohary H Yanikomeroglu 2019 Noncoherent MIMO signaling for block-fading channels: approaches and challenges *IEEE Veh. Technol. Mag.* 14 1 80 88
2. F Yuan S Jin Y Huang K Wong QT Zhang H Zhu 2015 Joint wireless information and energy transfer in massive distributed antenna systems *IEEE Commun. Mag.* 53 6 109 116
3. D Xia J Zhang S Dumitrescu 2013 Energy-efficient full diversity collaborative unitary space-time block code designs via unique factorization of signals *IEEE Trans. Inf. Theory* 59 3 1678 1703
4. BM Hochwald TL Marzetta TJ Richardson W Sweldens R Urbanke 2000 Systematic design of unitary space-time constellations *IEEE Trans. Inf. Theory* 46 6 1962 1973
5. LZ Zheng DNC Tse 2002 Communication on the Grassmann manifold: a geometric approach to the noncoherent multiple-antenna channel *IEEE Trans. Inf. Theory* 48 2 359 383
6. KG Seddik RH Gohary MT Hussien M Shaqfeh H Alnuweiri H Yanikomeroglu 2017 Multi-resolution multicasting over the grassmann and stiefel manifolds *IEEE Trans. Wirel. Commun.* 16 8 5296 5310
7. H Jafarkhani V Tarokh 2001 Multiple transmit antenna differential detection from generalized orthogonal designs *IEEE Trans. Inf. Theory* 47 6 2626 2631
8. D Kong X-G Xia T Jiang 2016 A differential QAM detection in uplink massive MIMO systems *IEEE Trans. Wirel. Commun.* 15 9 6371 6383
9. Y Wang Z Tian 2018 Multiple symbol differential detection for noncoherent communications with large-scale antenna arrays *IEEE Wirel. Commun. Lett.* 7 2 190 193
10. N Ishikawa S Sugiura 2017 Rectangular differential spatial modulation for open-loop noncoherent massive-MIMO downlink *IEEE Trans. Wirel. Commun.* 16 3 1908 1920
11. E Tsimballo RJ Piechocki A Nix 2017 Non-coherent MIMO scheme based on OFDM-MFSK *IEEE Wirel. Commun. Lett.* 6 3 406 409
12. A Elgam Y Balal Y Pinhasi 2021 Study of 5G-NR-MIMO links in the presence of an interferer *Electronics*. 10 6 732
13. Z Lin 2020 MIMO-FSK non-coherent detection with spatial multiplexing in fast-fading environment *J. China Univ. Posts Telecommun.* 27 5 47 54
14. RK Mallik RD Murch 2018 Optimal ASK levels for channel magnitude based diversity reception in rayleigh fading *IEEE Trans. Commun.* 66 9 4345 4360
15. A. Anttonen, A. Mammela and A. Kotelba, Error probability of energy detected multilevel PAM signals in lognormal multipath fading channels. In: *Proceedings of the IEEE International Conference on Communications (ICC)*, pp. 3883–3887 (2009)
16. GK Psaltopoulos A Wittneben 2010 Nonlinear MIMO: affordable MIMO technology for wireless sensor networks *IEEE Trans. Wirel. Commun.* 9 2 824 832
17. M Chowdhury A Manolakos A Goldsmith 2016 Scaling laws for noncoherent energy-based communications in the SIMO MAC *IEEE Trans. Inf. Theory* 62 4 1980 1992
18. A Manolakos M Chowdhury A Goldsmith 2016 Energy-based modulation for noncoherent massive SIMO systems *IEEE Trans. Wirel. Commun.* 15 11 7831 7846
19. F Gómez-Cuba M Chowdhury A Manolakos E Erkip AJ Goldsmith 2019 Capacity scaling in a non-coherent wide-band massive SIMO block fading channel *IEEE Trans. Wirel. Commun.* 18 12 5691 5704
20. Y-Y Zhang J-K Zhang H-Y Yu 2018 Physically securing energy-based massive MIMO MAC via joint alignment of multi-user constellations and artificial noise *IEEE J. Sel. Areas Commun.* 36 4 829 844
21. H Xie W Xu HQ Ngo B Li 2020 Non-coherent massive MIMO systems: a constellation design approach *IEEE Trans. Wirel. Commun.* 19 6 3812 3825
22. L You K-X Li J Wang X Gao X-G Xia B Ottersten 2020 Massive MIMO transmission for LEO satellite communications *IEEE J. Sel. Areas Commun.* 38 8 1851 1865
23. Y. Xiang, L. Milstein, Design of an ultra-low power MFSK system in the presence of jamming. In: *Proceedings of the 2021 IEEE Military Communications Conference (MILCOM)*, pp. 652–657 (2021)
24. Y Liu Q Zeng Y Zhao 2021 Novel channel-hopping pattern-based wireless IoT networks in smart cities for reducing multi-access interference and jamming attacks *J Wirel. Commun. Netw.* 2021 152
25. Z. Wang, L. Zheng, J. Chen, M. Lin and X. Deng, MIMO-MFSK spatial multiplexing in Rician channel with large doppler shift. In: *Proceedings of the IEEE 19th International Conference on Communication Technology (ICCT)*, pp. 649–652 (2019)
26. K Guan Z Zhong B Ai T Kürner 2014 Propagation measurements and analysis for train stations of high-speed railway at 930 MHz *IEEE Trans. Veh. Technol.* 63 8 3499 3516
27. CB Peel AL Swindlehurst 2004 Effective SNR for space-time modulation over a time-varying Rician channel *IEEE Trans. Commun.* 52 1 17 23
28. E Karami 2007 Tracking performance of least squares MIMO channel estimation algorithm *IEEE Trans. Commun.* 55 11 2201 2209
29. Y Fu C Wang A Ghazal EM Aggoune MM Alwakeel 2016 Performance investigation of spatial modulation systems under non-stationary wideband high-speed train channel models *IEEE Trans. Wirel. Commun.* 15 9 6163 6174
30. L Zhou Z Yang F Luan AF Molisch F Tufvesson S Zhou 2018 Dynamic channel model with overhead line poles for high-speed railway communications *IEEE Antennas Wirel. Propag. Lett.* 17 5 903 906

**Publisher's Note**

Springer Nature remains neutral with regard to jurisdictional claims in published maps and institutional affiliations.